

Research Article

Extraction of Saturation Current and Ideality Factor from Measuring V_{oc} and I_{sc} of Photovoltaic Modules

E. L. Meyer

University of Fort Hare, Institute of Technology, Private Bag X1314, Alice 5700, South Africa

Correspondence should be addressed to E. L. Meyer; emeyer@ufh.ac.za

Received 17 June 2017; Revised 7 September 2017; Accepted 27 September 2017; Published 19 December 2017

Academic Editor: K. R. Justin Thomas

Copyright © 2017 E. L. Meyer. This is an open access article distributed under the Creative Commons Attribution License, which permits unrestricted use, distribution, and reproduction in any medium, provided the original work is properly cited.

Saturation current (I_0) and ideality factor (n) of a p - n junction solar cell are an indication of the quality of the cell. These two parameters are usually estimated from dark current-voltage measurements. In this study, a quick and easy method to determine these two parameters by measuring open-circuit, V_{oc} , and short-circuit current, I_{sc} , is presented. Solar cell designers can use this method as a grading or diagnostic tool to evaluate degradation in photovoltaic (PV) modules. In order to verify the V_{oc} - I_{sc} method, a series of experiments have been conducted on a single cell and a 36-cell module. Good agreement between our V_{oc} - I_{sc} method and dark I-V measurements was obtained. An application of the method on the performance degradation of a single-junction a-Si:H module revealed that the module's I_0 increased by more than three orders of magnitude and n increased by 65% after an outdoor exposure of 130 kWh/m². This increase in n indicates that after exposure, the recombination current in the cells' space charge region increased due to the light-induced formation of metastable defects. The method is also used to assess the quality of five PV module technologies and proved to be reliable despite defective cells in a module.

1. Introduction

Photovoltaic (PV) cell or module saturation current (I_0) and ideality factor (n) are usually determined by fitting the Shockley equation to dark current-voltage (I-V) measurements. This is done by nonlinear parameter estimation software employing iterative methods. These methods require a minimum number of dark I-V points (100 in our case) measured very accurately in the microamp range. Photovoltaic research laboratories are more likely to have a solar simulator only and lack a high-cost semiconductor characterization system. Therefore, the capability of varying the irradiance in a simulator allows the extraction of ideality factor and recombination current. In this study, the relation between open-circuit voltage (V_{oc}) and short-circuit current (I_{sc}) of PV cells and modules has been investigated. By measuring V_{oc} and I_{sc} at different irradiance levels, a good linear correlation was found between these two parameters as expected from theoretical predictions. The interpretation of this linear relation is based on the assumption that the PV cells have

no significant shunt paths across their junction. In fact, it is shown that if the relation between V_{oc} and I_{sc} is not linear for a cell, the cell is expected to have significant shunt paths or low shunt resistances. Comparing results obtained from V_{oc} - I_{sc} measurements to dark I-V measurements indicate that the V_{oc} - I_{sc} method is a reliable and accurate way to quickly and easily determine the otherwise obscure parameters, I_0 and n . PV simulations were also used to verify the method, and I_0 and n obtained from the V_{oc} - I_{sc} method are in excellent agreement with the values of I_0 and n used in the simulations. Due to the simplicity of the method, it is a useful tool for grading cells and modules during manufacturing and also for analyzing any in-field degradation. This paper presents, verifies, and applies the V_{oc} - I_{sc} method used to determine a cell or module's saturation current and ideality factor.

2. Solar Cells: Operating Principles

Solar cells are diodes formed by joining n -type and p -type semiconductor materials. When forming this p - n junction,

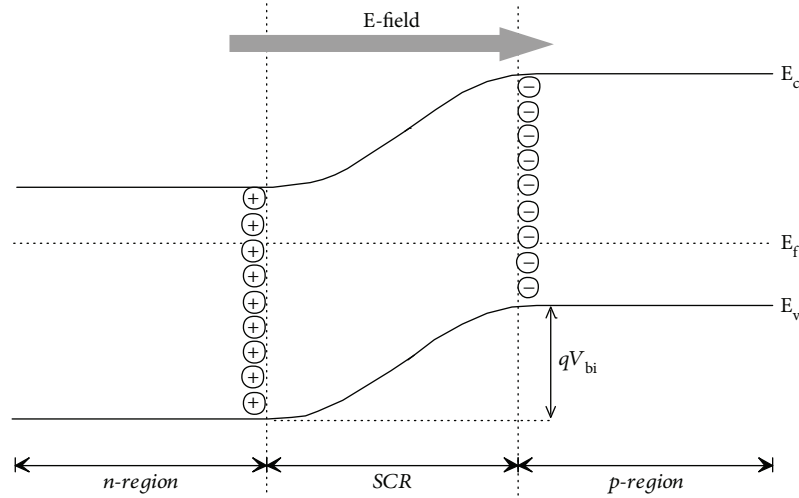


FIGURE 1: Energy band diagram of a p - n junction at thermal equilibrium.

electrons diffuse across the junction to the p -side where they recombine with holes. Similarly, holes diffuse across the junction to the n -side where they recombine with electrons giving rise to the diffusion component of the recombination current. On leaving the n -side, electrons leave behind positively ionized donor atoms and the holes leave behind negatively ionized acceptor atoms. These ionized atoms form a space charge region (SCR) giving rise to an electrical field directed from the n -type region towards the p -type region [1, 2]. The buildup of this electric field will, therefore, eventually oppose further diffusion of electrons and holes. At this condition, the Fermi levels in both regions are equal and the junction is said to be at thermal equilibrium. Figure 1 illustrates the energy band diagram of a p - n junction at thermal equilibrium. Also illustrated is the built-in potential barrier, V_{bi} , associated with the internal electric field.

2.1. Dark Current. When the p - n junction diode in Figure 1 is forward biased, the built-in potential barrier is lowered. Figure 2(a) shows the components of the recombination current when the junction is forward biased and Figure 2(b), the corresponding energy band diagram. The forward bias voltage, V , produces an injection of minority carriers into both sides, that is, electrons (filled circles) from the n -side into the p -side. The electrons in the p -side of the junction move by diffusion until they recombine with holes (empty circles). This recombination may take place either at the surface or in the bulk of the p -type material. This movement by diffusion of electrons in the p -side forms one component of the dark diode current (I_{D1}) in the solar cell. Similarly, the current resulting from diffusion of holes in the n -side is denoted by I_{D2} .

The total diffusion current in the n - and p -regions ($I_{D1} + I_{D2}$), which also constitutes ideal recombination, is given by the Shockley equation [2, 3]:

$$I_{D1} + I_{D2} = I_{01} \left[e^{qV/nkT} - 1 \right], \quad (1)$$

where I_{01} = reverse saturation current corresponding to the diffusion and recombination of electron and holes in the p - and n -regions, respectively; n = ideality factor = 1; k = Boltzmann's constant; T = absolute temperature.

The last component of the dark current is a result of recombination of electrons and holes in the SCR, I_{D3} . This current constitutes nonideal recombination and is given by

$$I_{D3} = I_{02} \left[e^{qV/nkT} - 1 \right], \quad (2)$$

where I_{02} = reverse saturation current corresponding to the generation and recombination of electron and holes in the SCR region; n = ideality factor > 1;

The total dark current comprises the components given in (1) and (2):

$$I_D = I_{01} \left[e^{qV/kT} - 1 \right] + I_{02} \left[e^{qV/nkT} - 1 \right]. \quad (3)$$

Equation (3) can be written as a single exponential formula:

$$I_D = I_0 \left[e^{qV/nkT} - 1 \right], \quad (4)$$

where I_0 = reverse saturation current governed by diffusion and recombination of electron and holes; $n=1$ if the dark current, I_D , is solely determined by diffusion; and $n>1$ if recombination in the SCR also contributes to I_D .

Apart from the recombination current given in (4), parasitic series and shunt resistances are also present in a practical solar cell. Figure 3 shows the equivalent circuit model of a p - n junction solar cell in the dark where the cell is forward biased by a variable power supply, V_{DC} . The shunt resistance, R_{sh} , represents any parallel high-conductivity paths across the junction or on the cell edges, and the series resistance, R_s , represents the resistance in the bulk of the material and in the Ohmic contacts [4–6].

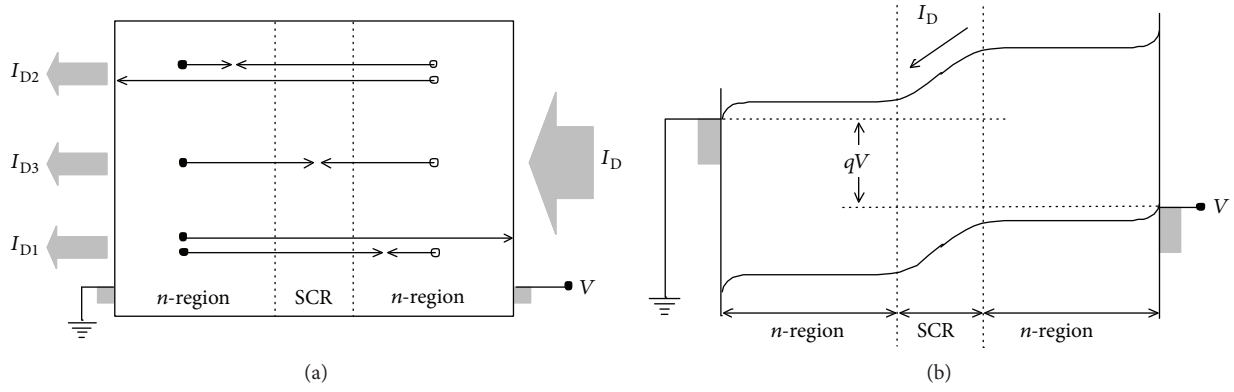


FIGURE 2: (a) Components of the recombination current in a forward biased p - n junction solar cell [2]. (b) Energy band diagram of a forward biased p - n junction corresponding to Figure 2(a).

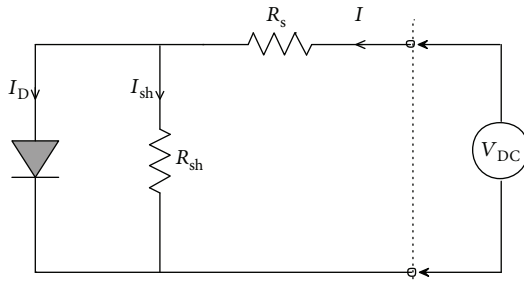


FIGURE 3: Equivalent circuit model of a practical solar cell with parasitic series and shunt resistances.

From the figure, it is evident that the current through the cell is given by

$$I = I_D + I_{sh}, \quad (5)$$

where I_D is given by (4) and I_{sh} is obtained from Kirchhoff's voltage rule. Substitution yields the equation governing the dark I-V characteristics of a cell or module:

$$I = I_0 \left[e^{qV/nkT} - 1 \right] + \frac{V - IR_s}{R_{sh}}. \quad (6)$$

2.2. Photogenerated Current. When the p - n junction solar cell is illuminated, the junction is forward biased and the cell produces a photogenerated current, I_{ph} . Figure 4(a) shows the equivalent circuit model of the illuminated solar cell and Figure 4(b) the corresponding energy band diagram when the illuminated cell is connected to a load.

The external current through the load, I , is given by [7]

$$I = I_{ph} - I_D - I_{sh}. \quad (7)$$

The equation governing the I-V characteristics of a PV cell or module is then given by

$$I = I_{ph} - I_0 \left[e^{qV/nkT} - 1 \right] - \frac{V - IR_s}{R_{sh}}. \quad (8)$$

The short-circuit current, I_{sc} , of the solar cell is obtained by setting V in (8) equal to zero and assuming that R_s is negligibly small; thus,

$$I_{sc} = I_{ph}. \quad (9)$$

Similarly, the cell's open-circuit voltage, V_{oc} , is obtained when no external current flows, that is, $I = 0$ in (8). Assuming that $I_0 \ll I_{sc}$ and $R_{sh} \gg V_{oc}/I_{sc}$, V_{oc} is then given by

$$V_{oc} = \frac{nkT}{q} (\ln I_{sc} - \ln I_0). \quad (10)$$

3. Validation of the V_{oc} - I_{sc} Method

From (10), it is evident that a plot of V_{oc} versus $\ln I_{sc}$ should be linear. The gradient of this linear plot allows the determination of ideality factor, n , and the y -intercept yields the reverse saturation current, I_0 :

$$n = \frac{\text{grad}}{kT/q}, \quad (11)$$

$$\ln I_0 = \frac{-y}{nkT/q}. \quad (12)$$

To verify the validity of (11), a series of experiments were conducted on a monocrystalline Si cell and a 36-cell multicrystalline Si module. A PV simulation program (PVSIM) [8] was also used to verify (11).

Equations (10) and (11) assume that the ideality factor is not influenced by irradiance levels and subsequently by voltage. This is however not the case. The ideality factor has a distinct dependence on voltage. This dependence is governed by unusual or nonideal recombination and parasitic series and shunt resistance. Figure 5(a) shows the theoretical dependence of ideality factor on voltage for an ideal solar cell and for a solar cell with parasitic resistances according to (8) [9]. In this calculation, $R_s = 0.100 \, \Omega \cdot \text{cm}^2$, $R_{sh} = 1.00 \, \text{M} \cdot \text{cm}^2$, $I_{01} = 1.00 \times 10^{-13} \, \text{A/cm}^2$ and $I_{02} = 1.00 \times 10^{-10} \, \text{A/cm}^2$. These are typical values for a Si p - n junction solar cell [10].

At low voltages (corresponding to very low irradiance levels), the ideality factor is governed by shunt paths across the p - n junction. At intermediate voltages, the ideality factor

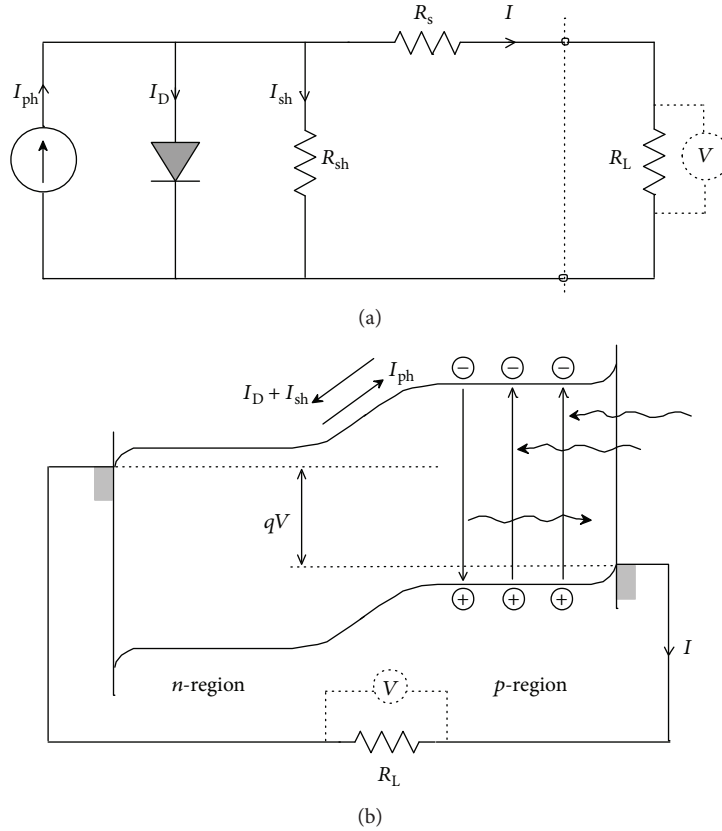


FIGURE 4: (a) Equivalent circuit model for an illuminated $p-n$ junction solar cell connected to a load. (b) Energy band diagram of an illuminated solar cell corresponding to Figure 4(a).

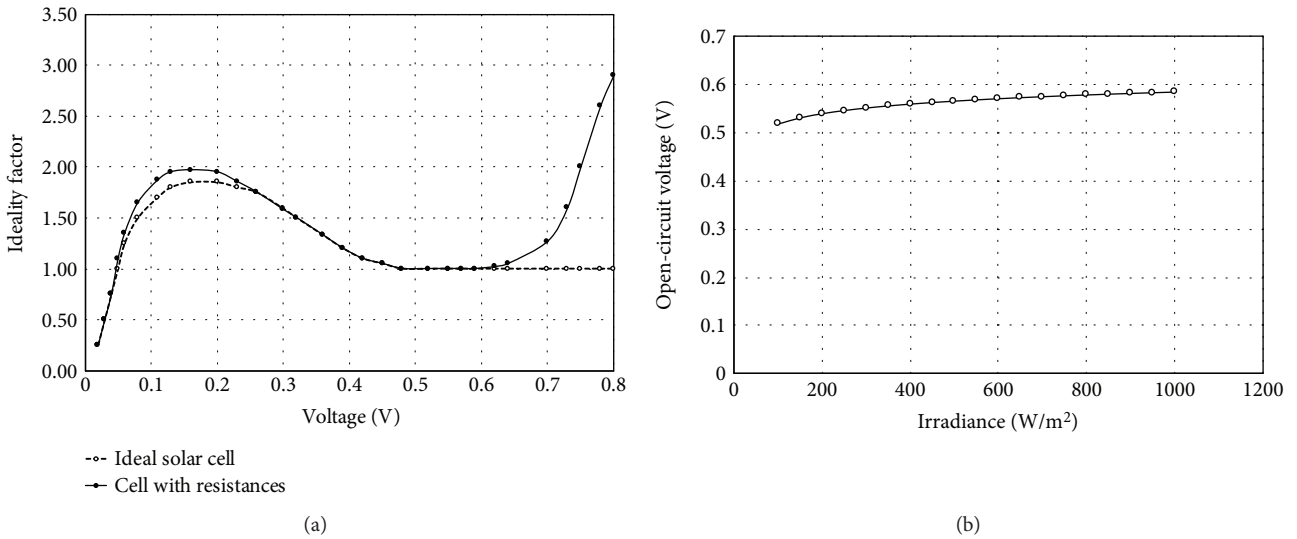


FIGURE 5: (a) Dependence of ideality factor on voltage across the junction. At low voltages, R_{sh} dominates the device performances, while at high voltages, R_s dominates. (b) Effect of irradiance on voltage across the cell. The measurements in this document are confined to between 169 W/m^2 and 1000 W/m^2 as governed by the physical setup of the experiment.

is very “stable”, and at high voltages (irradiance levels), it is governed by series resistances [9].

Figure 5(b) shows the dependence of voltage for our cell on irradiance level as obtained from PVSIM. From this figure, it is clear that the irradiance range that we are working

in results in a voltage range corresponding to the “stable” ideality factor region in Figure 5(a), that is between 0.5 V and 0.6 V. If the assumptions resulting in 10 ($I_0 \ll I_{sc}$ and $R_{sh} \gg V_{oc}/I_{sc}$) do not hold, then of course the ideality factor would not be “stable” in this voltage range. Therefore, this

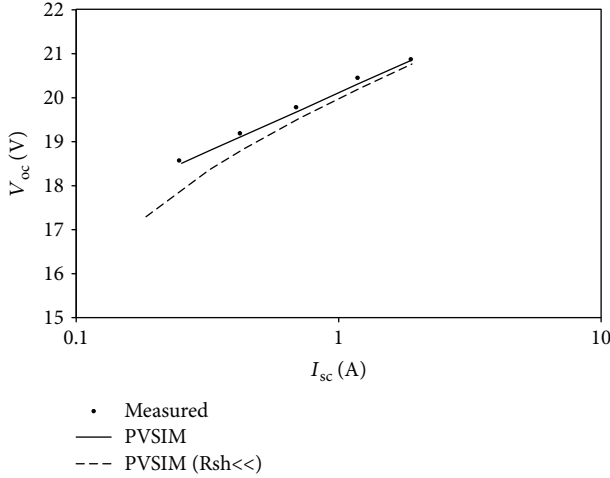


FIGURE 6: V_{oc} - I_{sc} data for the 36-cell module. The symbols indicate measured data and the solid line indicates simulations. Also shown is the effect of low cell shunt resistances on the relation between V_{oc} and I_{sc} (dashed line).

V_{oc} - I_{sc} method allows a qualitative measure of whether parasitic resistances are present or not as will be shown in Figure 6 below.

It should be noted that the light I-V measurements could only be done between irradiance levels of 169 W/m^2 and 1000 W/m^2 since the 4 clear mesh covers reduced the irradiance levels to specific values that could not be further altered. In this irradiance range, the voltage range corresponds to the region where the ideality factor is stable, provided that there are no parasitic resistances or nonideal recombination is taking place.

The advantage of the V_{oc} - I_{sc} method is that it will show that the assumptions in (10) are not met when the V_{oc} - I_{sc} curve is sublinear. Therefore, when the curve is sublinear, it is expected or suspected that the cell/module have shunting behavior, low series resistance, and/or nonideal recombination taking place.

3.1. Monocrystalline Si Cell. The diode ideality factor and saturation current can be accurately extracted by fitting (6) to a set of measured dark current-voltage (I-V) data using nonlinear parameter estimation software [11, 12]. In this study, we have used FitAll [13] to obtain estimates of n and I_0 from dark I-V measurements. Figure 7 shows the measured dark I-V data (symbols) and the nonlinear fit (solid line) of the monocrystalline Si cell. The standard deviation of the fit is 2.6×10^{-3} indicating that the parameters obtained are very good estimates of the true values. Table 1 lists the two parameters obtained from FitAll and their absolute deviations.

The I-V characteristics of the cell were then measured with a Spire-Sun 240A solar simulator at different irradiance levels (1000 W/m^2 , 614 W/m^2 , 375 W/m^2 , 229 W/m^2 , and 169 W/m^2) while the cell temperature was maintained at 25°C . Figure 8 shows the plot of V_{oc} versus $\ln I_{sc}$ measured at different irradiance levels. The correlation of the linear fit with the measured data is 99.84% indicating that

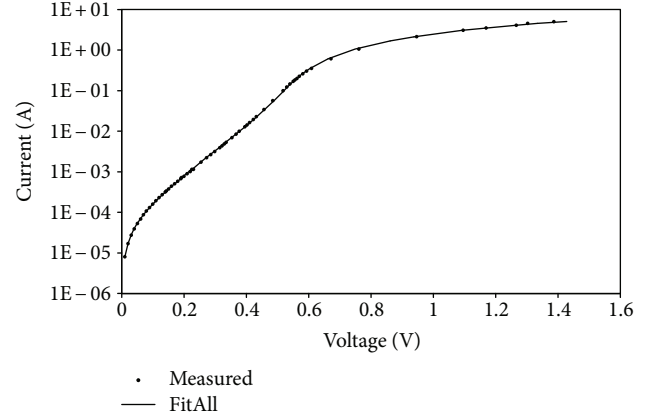


FIGURE 7: Dark current-voltage data of a mono-Si cell measured (symbols) and estimated (line) using FitAll.

TABLE 1: I_0 and n obtained from a nonlinear fit to measure dark I-V data of a single mono-Si cell.

Parameter	Estimated value	Absolute deviation (%)
I_0 (A)	5.39×10^{-5}	3.05×10^{-3}
n	2.83	0.03

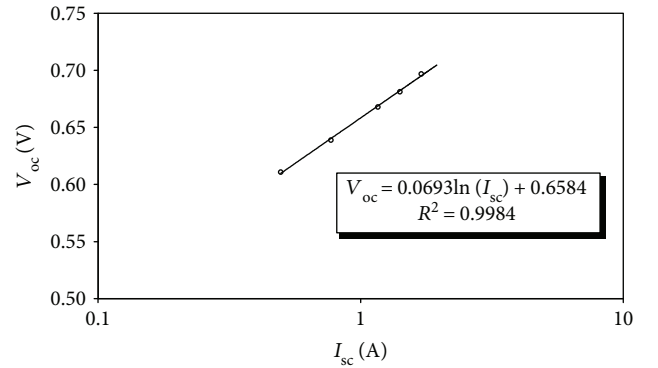


FIGURE 8: V_{oc} and I_{sc} measured (symbols) at different irradiance levels. The solid line is a linear fit.

the relation between V_{oc} and I_{sc} is in good accordance with the theoretical (10).

Table 2 lists the values obtained for I_0 and n from the linear fit and compares it to that obtained from the dark I-V measurements. Clearly, results obtained from the two methods (V_{oc} - I_{sc} method and dark I-V) are in good agreement. The relative error of the V_{oc} - I_{sc} method from the dark I-V results is 0.39 for recombination current I_0 and 0.05 for ideality factor n .

3.2. 36-Cell Multicrystalline Si Module. The method of extracting I_0 and n from V_{oc} - I_{sc} measurements was also used on a 36-cell multicrystalline Si module. The shunt resistance of the module was measured using an individual cell shunt measurement system [12]. No cells in the module had significantly low shunt resistances, and the total module shunt

TABLE 2: I_0 and n obtained from V_{oc} - I_{sc} measurements compared to that estimated from dark I-V measurements of the mono-Si cell.

Parameter	V_{oc} - I_{sc}	Dark I-V
I_0 (A)	7.48×10^{-5}	5.39×10^{-5}
n	2.70	2.83

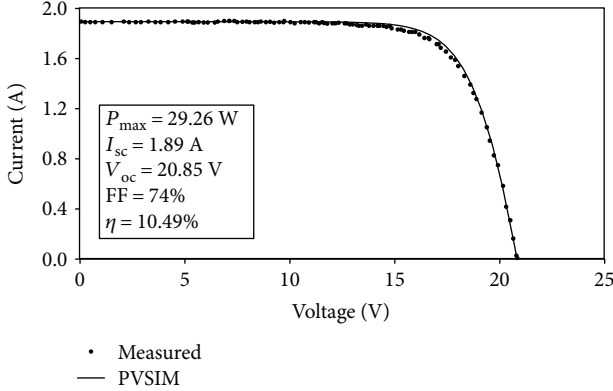


FIGURE 9: I-V characteristic of the 36-cell module measured (symbols) at STC and simulated (solid line) using PVSIM [8]. The performance parameters shown are those obtained from measurement.

TABLE 3: I_0 and n for the 36-cell module obtained from V_{oc} - I_{sc} measurements compared to that simulated using PVSIM.

Parameter	V_{oc} - I_{sc}	PVSIM
I_0 (A)	2.44×10^{-8}	3.08×10^{-8}
n	1.24	1.26

resistance was more than 10 M Ω . This value was confirmed by dark I-V measurements. Figure 9 shows the measured I-V characteristic (symbols) of the module and its performance parameters at standard test conditions (STC: 1000 W/m² irradiance, 25°C cell temperature and AM1.5 global spectrum). PVSIM [8] was then used to simulate (solid line), the module's characteristic at STC.

Figure 6 illustrates the relation between V_{oc} and I_{sc} of the measured and simulated data. The symbols are the measured data, the solid line the simulation, and the dashed line simulations of the same module but with low cell shunt resistances. The effect of the low cell shunt resistances is particularly evident at low irradiance levels. At these low levels, the assumption that $R_{sh} \gg V_{oc}/I_{sc}$ becomes invalid and the relation between V_{oc} and $\ln I_{sc}$ is sublinear. Therefore, if the relation between V_{oc} and $\ln I_{sc}$ is sublinear for a module or cell, one can conclude that the module or cell exhibits shunting behavior.

Values for I_0 and n obtained from both measured and simulated data are listed in Table 3. The good correlation between values obtained from measured and simulated data indicates that our method of extracting I_0 and n from V_{oc} - I_{sc} measurements is valid and accurate for both cells and

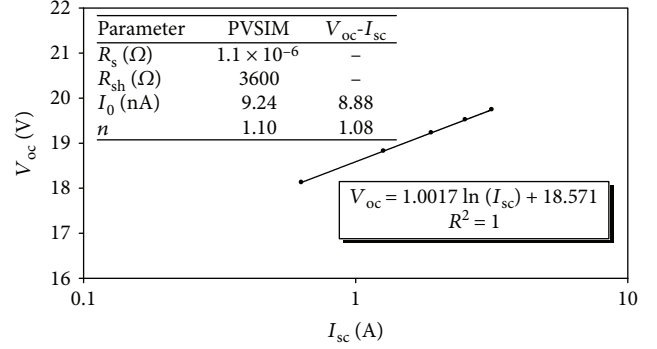


FIGURE 10: Relation between V_{oc} and I_{sc} of a 36-cell module simulated with PVSIM. The accompanying table lists the values of R_s , R_{sh} , I_0 , and n used in the simulations and compares I_0 and n with that obtained from the V_{oc} - I_{sc} method.

TABLE 4: Saturation current and ideality factor for a 14 Wp a-Si:H module obtained from V_{oc} - I_{sc} measurements.

Parameter	Exposure		
	0 kWh/m ²	80 kWh/m ²	130 kWh/m ²
I_0 (A)	5.47×10^{-9}	3.51×10^{-6}	2.59×10^{-5}
n	1.71	2.47	2.96

modules. The relative error of the V_{oc} - I_{sc} method from the PVSIM results is 0.21 for recombination current I_0 and 0.02 for ideality factor n .

3.3. Simulation of a 36-Cell Si Module. In the previous section, a PV simulation program (PVSIM) has been used to simulate the multicrystalline module. In this section, an arbitrary 36-cell module is simulated. The simulations are conducted for different irradiance levels from which V_{oc} - I_{sc} data points are obtained. Our method of extracting I_0 and n was then applied to these data points. The result is then compared to the values for I_0 and n used by PVSIM. Figure 10 shows the relation between the simulated V_{oc} and I_{sc} . Listed in the accompanying table are the values of R_s , R_{sh} , I_0 , and n used in the simulations. It is evident from this table that the values for I_0 and n obtained from the V_{oc} - I_{sc} method are in excellent agreement with I_0 and n used by PVSIM.

4. Application of the V_{oc} - I_{sc} Method

4.1. Degradation Analysis. Although the primary application of the V_{oc} - I_{sc} method is to obtain the obscure parameters of I_0 and n from I-V measurements in a solar simulator, the method can also be employed to establish and or confirm performance degradation when the tests are done periodically on modules deployed outdoors. In a study where a 14 Wp a-Si:H module was deployed outdoors [14], the module's performance degraded by about 60% after being exposed to 130 kWh/m². Our method was used to analyze this observed degradation. The module had an average individual cell shunt resistance of 100 Ω implying that the assumption $R_{sh} \gg V_{oc}/I_{sc}$ holds. Table 4 lists the values for I_0 and n

TABLE 5: Module technologies, rated power, STC-measured power, and aperture area efficiencies of the five modules used in the quality assessment.

Module technology	P_{\max} rated (W)	P_{\max} @ STC (W)	η (%)
CIS	10.0	10.76	9.19
a-Si:H	14.0	12.98	4.41
EFG-Si	32.0	31.64	11.3
Multi-Si	30.0	30.62	11.0
Mono-Si	65.0	64.45	10.7

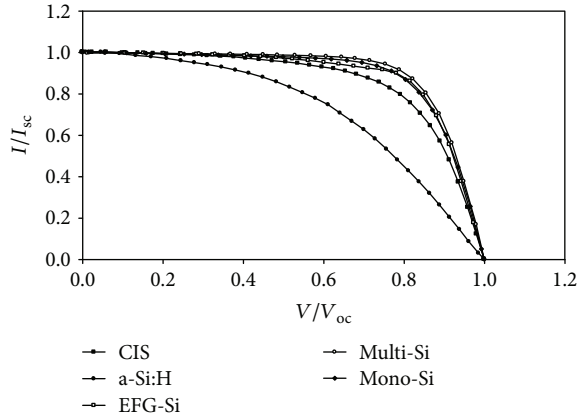


FIGURE 11: Normalized I-V characteristics of the five module technologies used.

obtained from V_{oc} - I_{sc} measurements before, during, and after a 180 kWh/m² outdoor exposure.

The increase in ideality factor implies that after each exposure, the recombination current in the SCR contributed more towards the dark current. This is also evident from the increase in the saturation current with exposure. When the a-Si:H cells are exposed to sunlight, the incoming photons generate electron-hole (e-h) pairs. When these e-h pairs recombine, a photon or phonon may be released. The emitted photons break the weak Si-Si bonds in the SCR. These broken bonds form metastable defects in the SCR, which enhances recombination there. The photons emitted from the enhanced recombination cause even more metastable defects to form and, thus, enhance recombination even more [15–18]. This increasing recombination, illustrated by I_0 in Table 5, deteriorates the performance and quality of the cells' junction since fewer carriers are now available for current transport in an external circuit.

4.2. Quality Assessment. The V_{oc} - I_{sc} method presented in this paper can be used to assess the quality of various modules. Because of its simplicity, module manufacturers, PV system designers, and researchers can use this method to quickly and easily assess module or cell quality. In this study, five modules comprising different module technologies were subjected to the V_{oc} - I_{sc} method. The modules are presented in Table 5 where the module technology, rated power, STC-

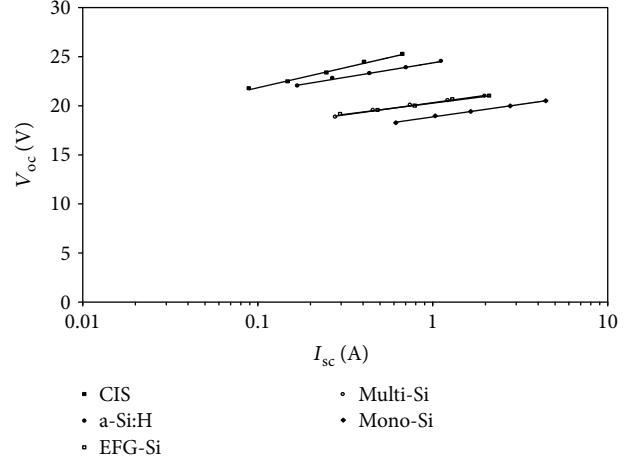


FIGURE 12: V_{oc} versus I_{sc} yielding ideality factor and reverse saturation current of the various module technologies.

TABLE 6: Parameters (n and I_0) obtained for various module technologies from V_{oc} - I_{sc} measurements.

Module	CIS	a-Si:H	EFG-Si	Multi-Si	Mono-Si
n	1.38	1.71	1.07	1.15	1.19
I_0 (nA)	486	5.47	1.28	5.82	40.7

measured power, and aperture area efficiencies are listed. Figure 11 shows the normalized I-V characteristics of the five modules measured at STC. The current values were normalized to I_{sc} and the voltage to V_{oc} . These normalized I-V characteristics enable direct comparison of the different module technologies. It is clear from the figure that the fill factor ($FF = P_{\max}/V_{oc}I_{sc}$) of the thin-film modules and hence their qualities are inferior to that of the crystalline modules.

The V_{oc} - I_{sc} method was used to assess module quality in terms of I_0 and n . Figure 12 shows V_{oc} as a function of I_{sc} for the five module technologies. Different values for V_{oc} and I_{sc} were obtained by measuring I-V characteristics at various irradiance levels inside the solar simulator. Module temperatures were maintained at 25°C.

Table 6 lists the parameters (n and I_0) obtained from the logarithmic fits to the data in Figure 11. These values were confirmed with dark I-V measurements. The closer n is to unity, the better the quality of the module cells. Also, $n > 1$ implies that apart from ideal recombination in the quasi-neutral p - and n -regions, nonideal recombination also takes place in the space charge region (SCR) of the p - n junction [2]. From the table, it is evident that the EFG-Si module has the best quality cells. This is contrary to the normalized I-V characteristics in Figure 10, which suggests that the multicrystalline module has the highest FF and, hence, the best quality. The lower FF of the EFG-Si module in Figure 10 is, however, attributed to a crack on one of its cells. Therefore, the V_{oc} - I_{sc} method still gives accurate results even when light I-V measurements may be misleading.

The relatively higher n for the thin-film modules reveals that their cell quality is lower than the crystalline cells. It also implies that nonideal recombination takes place especially

for the a-Si:H module with n close to 2. The high I_0 of the CuInSe₂ (CIS) module is due to the fact that the CIS module showed shunting behavior [14, 19–22] implying that the ratio V_{oc}/I_{sc} approaches R_{sh} . In general, the lower quality of the thin-film modules is mainly due to less stringent manufacturing processes used in an attempt to reduce manufacturing costs.

5. Summary and Conclusions

In this paper, it has been successfully shown that the saturation current, I_0 , and the ideality factor, n , of cells and modules can be extracted from measuring V_{oc} and I_{sc} at different irradiance levels. In comparison to dark I-V measurements and simulations, the underlying physics and implementation of our method are much simpler and in good correlation with results obtained from both dark I-V measurements and simulations. The assumption $R_{sh} \gg V_{oc}/I_{sc}$ is generally true for cells and modules. If the relation between V_{oc} and $\ln I_{sc}$ is sublinear for a cell or module, it can be concluded that the cell or module exhibits shunting behavior.

Due to its simplicity, our method can be used in any PV laboratory with a simulator as well as outdoors. These outdoor measurements would involve the physical measurements of V_{oc} and I_{sc} with an appropriate multimeter and place clear mesh layers over the modules to vary the incident irradiance on the modules. If the module temperature also varies, corrections need to be made for that. It can also be used on measurements taken outdoors with common laboratory equipment [23]. To the cell and module designer, it is a quick and useful diagnostic tool to grade the quality of cells and modules. This V_{oc} - I_{sc} method has also been used in this study to analyze the degradation in an a-Si:H module deployed outdoors. The saturation current of the module increased by more than three orders of magnitude and the ideality factor increased by 65% from 1.71 initially to 2.83 after the 130 kWh/m² exposure. These results confirmed the Staebler-Wronski effect where the formation of recombination centers in the SCR is enhanced by exposure to light photons. Assessment of the quality of various module technologies revealed that the thin-film module technologies are inferior in quality compared to crystalline Si modules. The V_{oc} - I_{sc} method also proved to be reliable even when there are defective cells in a module, which causes results obtained from light I-V measurements to be misleading.

Conflicts of Interest

The authors declare that there is no conflict of interest regarding the publication of this paper.

Acknowledgments

The authors wish to express their gratitude to the Govan Mbeki Research and Development Centre at the University of Fort Hare, the National Research Foundation of South Africa, and Eskom for their financial support.

References

- [1] L. Li, P. A. Salvador, and G. S. Rohrer, "Photocatalysts with internal electric fields," *Nanoscale*, vol. 6, no. 1, pp. 24–42, 2014.
- [2] E. Lorenzo, *Solar Electricity: Engineering of Photovoltaic Systems*, P. Davies, Ed., PROGNSA, 1994.
- [3] J. Cubas, S. Pindado, and C. de Manuel, "Explicit expressions for solar panel equivalent circuit parameters based on analytical formulation and the Lambert W-function," *Energies*, vol. 7, no. 7, pp. 4098–4115, 2014.
- [4] M. A. Green, *Solar Cells: Operating Principles, Technology and System Application*, University of New South Wales, 1992.
- [5] G. Sahin, "Effect of temperature on the series and shunt resistance of a silicon solar cell under frequency modulation," *Journal of Basic and Applied Physics*, vol. 5, no. 1, pp. 21–29, 2016.
- [6] R. Kisslinger, W. Hua, and K. Shankar, "Bulk heterojunction solar cells based on blends of conjugated polymers with II–VI and IV–VI inorganic semiconductor quantum dots," *Polymers*, vol. 9, no. 2, p. 35, 2017.
- [7] J. A. Mazer, *Solar Cells: An Introduction to Crystalline Photovoltaic Technology*, Kluwer Academic Publications, 1997.
- [8] D. L. King, J. K. Dudley, and W. E. Boyson, "PVSIM: a simulation program for photovoltaic cells, modules and arrays," in *Proceedings of the 25th IEEE PV Specialists Conference*, pp. 1295–1297, 1996.
- [9] S. J. Robinson et al., *12th EU PVSEC*, p. 1831, 1994.
- [10] A. Nussbaum, "Generation-recombination characteristic behavior of silicon diodes," *Physica Status Solidi (a)*, vol. 19, no. 2, pp. 441–450, 1973.
- [11] D. L. King and J. A. Hansen, "Dark current-voltage measurements on photovoltaic modules as a diagnostic or manufacturing tool," in *Proceedings of the 26th IEEE PV Specialists Conference*, pp. 1125–1128, 1997.
- [12] E. L. Meyer and E. E. van Dyk, "Assessing the reliability and degradation of photovoltaic module performance parameters," *IEEE Transaction on Reliability*, vol. 53, no. 1, pp. 83–92, 2004.
- [13] MTR Software, *FitAll Nonlinear Regression Analysis: Research Edition*, pp. 130–141, 1998, (Function Reference).
- [14] E. L. Meyer and E. E. van Dyk, "Characterization of degradation in thin-film photovoltaic module performance parameters," *Renewable Energy Journal*, vol. 28, no. 9, pp. 1455–1469, 2003.
- [15] D. L. Staebler and C. R. Wronski, "Reversible conductivity changes in discharge-produced amorphous Si," *Applied Physics Letters*, vol. 31, no. 4, pp. 292–294, 1977.
- [16] A. Kołodziej, "Staebler-Wronski effect in amorphous silicon and its alloys," *Opto-Electronics Review*, vol. 12, no. 1, pp. 21–32, 2004.
- [17] T. Shimizu, "Staebler-Wronski effect in hydrogenated amorphous silicon and related alloy films," *Japanese Journal of Applied Physics*, vol. 43, no. 6A, pp. 3257–3268, 2004.
- [18] F. Kohler, T. Zimmermann, S. Muthmann, A. Gordijn, and R. Carius, "Structural order and Staebler-Wronski effect in hydrogenated amorphous silicon films and solar cells," *IEEE Journal of Photovoltaics*, vol. 4, no. 1, pp. 4–9, 2014.
- [19] E. L. Meyer and E. E. van Dyk, "Analysis of degradation in CuInSe₂ photovoltaic modules," *Physica status solidi (a)*, vol. 201, no. 10, pp. 2245–2250, 2004.
- [20] S. Ahn, K. Kim, A. Cho et al., "CuInSe₂ (CIS) thin films prepared from amorphous Cu-In-Se nanoparticle precursors for

solar cell application,” *ACS Applied Materials & Interfaces*, vol. 4, no. 3, pp. 1530–1536, 2012.

- [21] K. W. Mitchell, W. Chesarek, D. R. Willett, C. Eberspacher, J. H. Ermer, and R. R. Gay, “CuInSe₂ photovoltaic modules,” *Solar Cells*, vol. 30, no. 1–4, pp. 131–136, 1991.
- [22] E. L. Meyer and E. E. van Dyk, “Analysis of the effect of parasitic resistances on the performance of photovoltaic modules,” *Renewable Energy*, vol. 29, no. 3, pp. 333–344, 2004.
- [23] E. L. Meyer and E. E. van Dyk, “Monitoring I_{sc} , V_{oc} and performance parameters of photovoltaic modules,” in *Proceedings of the 17th European Photovoltaic Solar Energy Conference*, Germany, 2001, Munich.

